
## Emergent 3×3 charge order on the Cs reconstruction of kagome superconductor $CsV_3Sb_5$

Xianghe Han(韩相和), Zhongyi Cao(曹钟一), Zihao Huang(黄子豪), Zhen Zhao(赵振), Haitao Yang(杨海涛), Hui Chen(陈辉), and Hong-Jun Gao(高鸿钧)

**Citation:**Chin. Phys. B, 2025, 34 (**1**): 016801. DOI: 10.1088/1674-1056/ad8fa1

**What follows is a list of articles you may be interested in**

---

## Surface evolution of thermoelectric material $KCu_4Se_3$ explored by scanning tunneling microscopy

Yumin Xia(夏玉敏), Ni Ma(马妮), Desheng Cai(蔡德胜), Yuzhou Liu(刘宇舟), Yitong Gu(谷易通), Gan Yu(于淦), Siyu Huo(霍思宇), Wenhui Pang(庞文慧), Chong Xiao(肖翀), and Shengyong Qin(秦胜勇)

Chin. Phys. B, 2024, 33 (**8**): 086804. DOI: 10.1088/1674-1056/ad50c4

## Cryogenic transmission electron microscopy on beam-sensitive materials and quantum science

Gang Wang(王刚) and Jun-Hao Lin(林君浩)

Chin. Phys. B, 2024, 33 (**8**): 086801. DOI: 10.1088/1674-1056/ad5af0

## A first-principles study on remote van der Waals epitaxy through a graphene monolayer on semiconductor substrates

Rui Hou(侯锐) and Shenyuan Yang(杨身园)

Chin. Phys. B, 2023, 32 (**6**): 066801. DOI: 10.1088/1674-1056/ac92d6

## Reconstruction and stability of $Fe_3O_4$(001) surface: An investigation based on particle swarm optimization and machine learning

Hongsheng Liu(柳洪盛), Yuanyuan Zhao(赵圆圆), Shi Qiu(邱实), Jijun Zhao(赵纪军), and Junfeng Gao(高峻峰)

Chin. Phys. B, 2023, 32 (**5**): 056802. DOI: 10.1088/1674-1056/acb9e4

## Molecular beam epitaxy growth of monolayer hexagonal $MnTe_2$ on Si(111) substrate

S Lu(卢帅), K Peng(彭坤), P D Wang(王鹏栋), A X Chen(陈爱喜), W Ren(任伟), X W Fang(方鑫伟), Y Wu(伍莹), Z Y Li(李治云), H F Li(李慧芳), F Y Cheng(程飞宇), K L Xiong(熊康林), J Y Yang(杨继勇), J Z Wang(王俊忠), S A Ding(丁孙安), Y P Jiang(蒋烨平), L Wang(王利), Q Li(李青), F S Li(李坊森), and L F Chi(迟力峰)

Chin. Phys. B, 2021, 30 (**12**): 126804. DOI: 10.1088/1674-1056/ac2e63

---

**SPECIAL TOPIC — Recent progress on kagome metals and superconductors**

# Emergent 3×3 charge order on the Cs reconstruction of kagome superconductor $CsV_3Sb_5$

Xianghe Han(韩相和)[1,2], Zhongyi Cao(曹钟一)[1,2], Zihao Huang(黄子豪)[1,2], Zhen Zhao(赵振)[1,2], Haitao Yang(杨海涛)[1,2,3], Hui Chen(陈辉)[1,2,3,‡], and Hong-Jun Gao(高鸿钧)[1,2,3,†]

[1] *Beijing National Center for Condensed Matter Physics and Institute of Physics, Chinese Academy of Sciences, Beijing* 100190, *China*
[2] *School of Physical Sciences, University of Chinese Academy of Sciences, Beijing* 100049, *China*
[3] *Hefei National Laboratory, Hefei* 230088, *China*

(Received 28 September 2024; revised manuscript received 2 November 2024; accepted manuscript online 7 November 2024)

The alkali adatoms with controlled coverage on the surface have been demonstrated to effectively tune the surface band of quantum materials through *in situ* electron doping. However, the interplay of orderly arranged alkali adatoms with the surface states of quantum materials remains unexplored. Here, by using low-temperature scanning tunneling microscopy/spectroscopy (STM/S), we observed the emergent 3×3 super modulation of electronic states on the $\sqrt{3}\times\sqrt{3}R30^\circ$ (R3) Cs ordered surface of kagome superconductor $CsV_3Sb_5$. The nondispersive 3×3 superlattice at R3 ordered surface shows contrast inversion in positive and negative differential conductance maps, indicating a charge order origin. The 3×3 charge order is suppressed with increasing temperature and undetectable at a critical temperature of ∼ 62 K. Furthermore, in the Ta substituted sample $CsV_{2.6}Ta_{0.4}Sb_5$, where long-range 2×2×2 charge density wave is significantly suppressed, the 3×3 charge order on the R3 ordered surface becomes blurred and much weaker than that in the undoped sample. It indicates that the 3×3 charge order on the R3 ordered surface is directly correlated to the bulk charge density waves in $CsV_3Sb_5$. Our work provides a new platform for understanding and manipulating the cascade of charge orders in kagome superconductors.

**Keywords:** $CsV_3Sb_5$, surface reconstruction, alkali atoms, charge order, scanning tunneling microscope/spectroscopy

**PACS:** 68.37.Ef, 68.37.Ps, 81.15.–z, 81.05.Zx

**DOI:** 10.1088/1674-1056/ad8fa1 **CSTR:** 32038.14.CPB.ad8fa1

## 1. Introduction

Alkali metal atoms have been demonstrated to play a crucial role for manipulating the intriguing physics in quantum materials. When deposited on the surface of a layered material, alkali metal atoms could either diffuse on the surface or intercalate into the van der Waals gaps of the substrate. On one hand, the intercalation of the alkali atoms, which usually takes place in materials with large interlayer space (i.e., transition metal dichalcogenides), effectively decouples the first layer from the bulk, causing a 3D-to-2D transition and providing platforms for studying materials in the 2D limit.[1–3] On the other hand, the alkali atoms adsorbing on the surface introduce an electron doping effect. Charge transfer from the alkali atoms to the substrate results in various surface band filling levels.[4] In superconductors, the doping effect can significantly enhance superconductivity at an optimal coverage, possibly due to the enhanced electron–phonon coupling.[5–10] Continuous *in situ* deposition of alkali atoms allows precise control of the doping effect, which further achieves the evolution of Fermi surface and drives phase transition of quantum materials.[11,12] Interestingly, unlike the randomly distributed alkali adatoms, the ordering of absorbed alkali atoms on the surface provides a new way for tuning and creating quantum states, such as realization of the solid-state quantum simulator emulating molecular orbitals at semiconductor surfaces[13] and emergence of surface superconductivity.[14]

The layered kagome family $AV_3Sb_5$ ($A$ = K, Rb or Cs) and its derivatives exhibit a cascade of intriguing quantum states including charge density waves,[15–22] electronic nematicity,[23–27] smectic order,[21,28,29] pair density waves,[30–32] superconductivity,[33–39] and possible Majorana zero mode.[40,41] Despite these intriguing phenomena, precise manipulation of the quantum states and emergence of novel phenomena still remain to be fully explored. To this end, the role of alkali atoms in the cascade of electronics states in $AV_3Sb_5$ has been studied. When the bulk $CsV_3Sb_5$ is exfoliated to less than 5 layers, the significant loss of surface Cs may affect the CDW and superconductivity.[42] The external metal atom can be trapped by an alkali adatom, forming a symmetry-breaking diatomic rotor at the Sb surface.[43] Photoemission spectroscopic study of $A$ and Sb terminations of $AV_3Sb_5$ shows different polarity and opposite doping nature.[44,45] Cs dosing on to $CsV_3Sb_5$ first increases electron filling[46] which

†Corresponding author. E-mail: hjgao@iphy.ac.cn
‡Corresponding author. E-mail: hchenn04@iphy.ac.cn

fully suppresses the CDW state. Further dosing alkali atoms onto the kagome superconductor $AV_3Sb_5$ results in the growth of alkali thin films, which will finally grow into a fcc structure from the bcc one in the bulk.[47] Except for the electron doping effect of randomly distributed alkali adatoms, the orderly arranged alkali atoms could induce extra symmetry breaking on the surface. Although multiple reconstructions with different doping levels were reported,[48] the interplay of ordered alkali surfaces of kagome superconductors with the symmetry breaking quantum states remains elusive.

Here, by using low-temperature scanning tunneling microscopy/spectroscopy (STM/S), we observed a 3×3 charge order on the $\sqrt{3}\times\sqrt{3}R30^\circ$ (R3) Cs ordered surface of $CsV_3Sb_5$. This order is non-dispersive in a large range of energy and the $\mathrm{d}I/\mathrm{d}V$ maps taken at opposite energies (e.g., ±50 meV) show contrast inversion. The intensity of the 3×3 charge order is weakened with increasing temperature and the critical temperature extracted by fitting is about 62 K. In addition, in the Ta doped $CsV_{2.6}Ta_{0.4}Sb_5$ sample where the 2×2×2 CDWs in pristine sample are significantly suppressed, the intensity of the 3×3 charge order becomes weaker, which implies that the emergent charge order is directly correlated with the bulk CDWs.

## 2. Methods

The $CsV_3Sb_5$ and Ta doped samples were grown via a modified self-flux method.[17,30] The samples used in the experiments were cleaved at about 80 K and immediately transferred to an STM chamber. Experiments were performed in an ultrahigh-vacuum ($1\times10^{-10}$ mbar) low-temperature (420 mK) STM system equipped with a vertical 11 T magnetic field. All the scanning parameters (setpoint voltage and current) of the STM topographic images are listed in the figure captions. Tungsten tips used in the experiment were fabricated via electrochemical etching and calibrated on a clean Au(111) surface prepared by repeated cycles of sputtering with argon ions and annealing at 500 °C.

## 3. Results and discussion

The layered kagome superconductor $CsV_3Sb_5$ ($T_c\sim$ 2.3 K) shows a hexagonal symmetry structure with a kagome lattice consisting of V atoms (Fig. 1(a)). Cleavage produces two types of surfaces, i.e., Cs and Sb surfaces. The Sb surface shows the honeycomb lattice with a lattice constant of ∼ 0.54 nm, which is consistent with the crystal lattice constant.[30] Meanwhile, the Cs terminated surface shows various reconstructions due to the low diffusion barriers of Cs adatoms on Sb surfaces. The dominant reconstructed surface is $\sqrt{3}\times\sqrt{3}R30^\circ$ (R3) Cs reconstruction. In such reconstructed surface, the Cs–Cs distance in R3 is about 0.935 nm and the lattice rotates 30° from the pristine lattice (Fig. 1(c)).

There are two main topographic features of the R3 reconstructed surfaces. (1) There are randomly distributed domain walls connecting various R3 domains, exhibiting dark line defects in the large-scale STM images (Fig. 1(d)). The atomically-resolved STM images show the domain walls correspond to the boundary of two R3 domains with a phase shift (Fig. 1(d)). (2) There are also some protrusions in the R3 reconstructed surface regions (Fig. 1(b)). Based on the high resolution STM images, we attribute these protrusions to triangle-shaped tetramer with the nearest Cs–Cs distance of ∼ 0.54 nm (Fig. 1(e)). The low energy electron states of the R3 Cs reconstruction show a broad peak around 25 meV (Fig. 1(f)), and the modest difference can be observed between the $\mathrm{d}I/\mathrm{d}V$ spectra of R3 Cs reconstruction and Sb surface, indicating possible novel electronic states in the R3 Cs reconstruction.

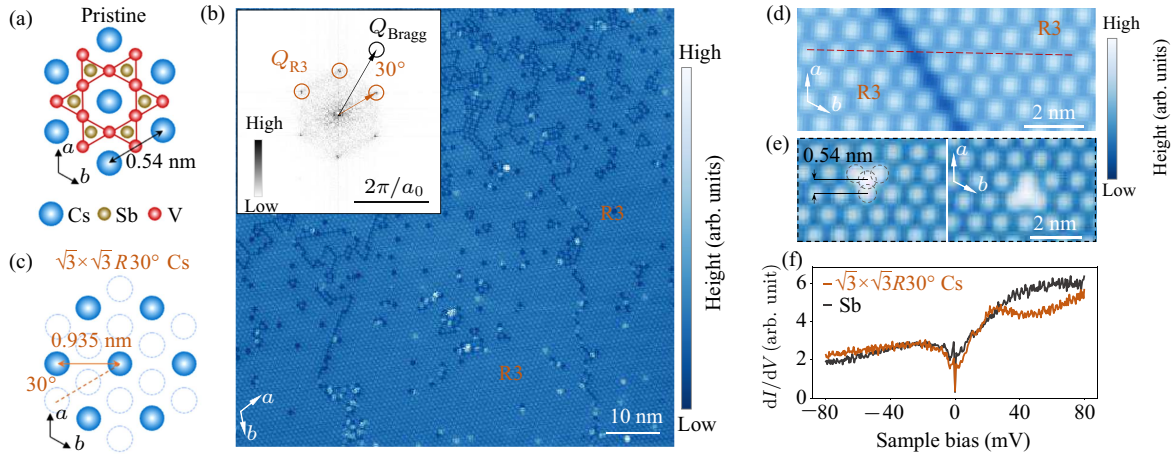


**Fig. 1.** Atomic model and STM image of the $\sqrt{3}\times\sqrt{3}R30^\circ$ Cs ordered surface of $CsV_3Sb_5$. (a) Top view (*ab* plane) of the atomic model of $CsV_3Sb_5$, showing the hexagonal Cs lattice with a constant of 0.54 nm. (b) Large-scale STM image of the $\sqrt{3}\times\sqrt{3}R30^\circ$ (short for R3) Cs ordered surface ($V_{set}=900$ mV, $I_t=50$ pA). Inset: the Fourier transform (FT) of STM image, showing the peaks of pristine crystalline lattice, $\boldsymbol{Q}_{Bargg}$ (black circle) and R3 superlattice, $\boldsymbol{Q}_{R3}$ (brown circle). (c) Schematic of the R3 Cs reconstruction, illustrating that the nearest Cs–Cs distance (approximately 0.935 nm) is $\sqrt{3}$ times the pristine lattice constant (0.54 nm) and the lattice is oriented at 30° with respect to the pristine crystalline lattice. (d) Atomically-resolved STM image of the characteristic domain boundary in R3 reconstruction, showing a phase shift between two domains of the R3 superlattice ($V_{set}=900$ mV, $I_t=50$ pA). (e) Atomically-resolved STM image of the Cs tetramer ($V_{set}=600$ mV, $I_t=500$ pA), showing that the distance between the nearest Cs atoms is 0.54 nm. (f) $\mathrm{d}I/\mathrm{d}V$ spectra of the Sb surface and R3 reconstruction at 0.4 K, showing a sharper gap edge at the positive energy side in the R3 spectrum. $V_{set}=100$ mV, $I_t=2$ nA, $V_{mod}=0.3$ mV.

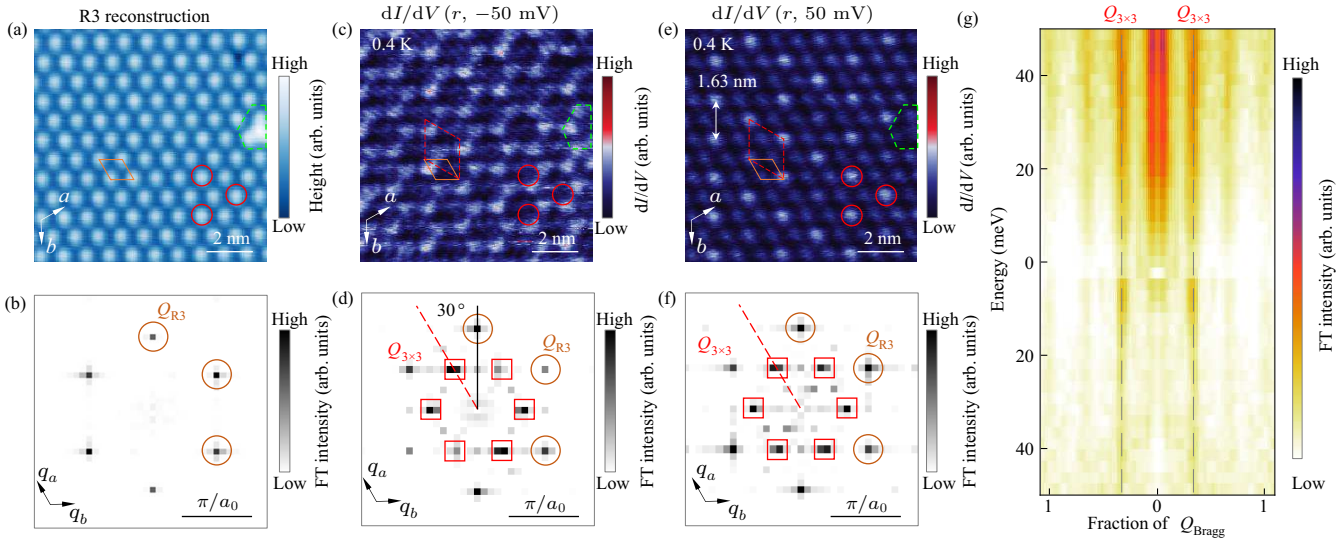


**Fig. 2.** Observation of $3\times3$ charge order on R3 reconstructed surface. (a) and (b) STM image and corresponding FT pattern of a typical R3 reconstructed surface ($V_{\mathrm{set}} = 50$ mV, $I_{\mathrm{t}} = 400$ pA), showing a uniform R3 lattice (highlighted by the brown circles in (b)). (c) and (e) d$I$/d$V$ maps taken at ±50 mV of the same region in (a) at 0.4 K, showing the $3\times3$ superlattice modulation (red rectangles) and intensity contrast in the differential conductance maps (red circles in (c) and (e)). The Cs tetramer marked by the green dashed line is a marker for the d$I$/d$V$ maps of the same region. (d) and (f) Corresponding Fourier transforms of d$I$/d$V$ maps in (c) and (e), with $\boldsymbol{Q}_{\mathrm{R3}}$ and $\boldsymbol{Q}_{3\times3}$ marked by brown circles and red rectangles, respectively and a 30° angle between them. (g) Energy dependence of the FT cut along the dashed red line in (d), showing that the vector at $\boldsymbol{Q}_{3\times3}$ is non-dispersive. For all d$I$/d$V$ data in this figure, $V_{\mathrm{set}} = 50$ mV, $I_{\mathrm{t}} = 400$ pA, $V_{\mathrm{mod}} = 2$ mV.

We then study the electronic states of R3 ordered Cs reconstruction. We select a 10 nm×10 nm R3 ordered Cs surface region without line defects (Fig. 2(a)). In the Fourier transform (Fig. 2(b)) of the STM image in Fig. 2(a), there are only six peaks from R3 reconstructions ($\boldsymbol{Q}_{\mathrm{R3}}$). The 2×2 and 1×4 CDWs are undetectable in the R3 reconstruction, which is consistent with previous works.[30,48] In contrast, in the d$I$/d$V$ maps at low energy range of the same region in Fig. 2(a), a new superlattice with a 30° rotation from $\boldsymbol{Q}_{\mathrm{R3}}$ (highlighted by the red rectangles) is observed (Figs. 2(c) and 2(d)). The periodicity of the emergent superlattice is $\sqrt{3}$ longer than that of R3 reconstruction, which means a $3\times3$ superlattice aligns with the pristine lattice ($\boldsymbol{Q}_{3\times3}$). The $\boldsymbol{Q}_{3\times3}$ superlattice is observed in the d$I$/d$V$ maps at a large range of energies. Furthermore, there is a contrast inversion between two maps at opposite energies (red circles in Figs. 2(c) and 2(e)). In the energy dependent cut line along the red dashed line in Fig. 2(d), the dominant signal locates at the length of 1/3 $\boldsymbol{Q}_{\mathrm{Bragg}}$ and it is non-dispersive (Fig. 2(g)). Consequently, we ascribe the emergent superlattice in d$I$/d$V$ maps to a $3\times3$ charge order (Figs. 2(d) and 2(f)).

We next investigate the temperature evolution of emergent $3\times3$ charge order on the R3 reconstruction. In both superconducting (0.4 K, Figs. 2(c) and 2(e)) and normal states (4.2 K, Fig. 3(a)), the $3\times3$ charge order is observed. When the temperature $T = 10$ K, the intensities of the R3 peaks remain nearly unchanged while the $3\times3$ charge order is suppressed (Fig. 3(b)). We thus plot the average intensity of three $\boldsymbol{Q}_{3\times3}$ peaks with increasing temperature (Fig. 3(c)). To exclude the tip effect and other measurement conditions, we normalize the $\boldsymbol{Q}_{3\times3}$ intensity with the averaged noise background. In contrast to the random variation near an average value for the $\boldsymbol{Q}_{\mathrm{R3}}$ peaks, the intensity of the $\boldsymbol{Q}_{3\times3}$ peaks in the FT gradually decrease with increasing temperature. The evolution of the $3\times3$ peak intensity with temperature is well fitted by an exponential function (Fig. 3(c)), where the critical temperature for the $3\times3$ charge order is determined to be about 60 K.

Finally, we study the correlation between the emergent $3\times3$ charge order and the three-dimensional CDWs in $CsV_3Sb_5$. For comparison with the pristine $CsV_3Sb_5$ where long-range $2\times2$ and $1\times4$ CDWs are observed with the absence of $\boldsymbol{Q}_{3\times3}$ at Sb surfaces (Fig. 4(a)), we intentionally choose $CsV_{2.6}Ta_{0.4}Sb_5$ in which the long-range CDWs are undetectable as shown in the STM image of Sb surface (Fig. 4(b)). Like in the pristine $CsV_3Sb_5$, we observe R3 reconstruction on the surfaces of the Ta doped $CsV_3Sb_5$ (Fig. 4(c)). In the d$I$/d$V$ maps of R3 reconstruction, the $3\times3$ peaks become much weaker than that of pristine $CsV_3Sb_5$ at the same energy (Figs. 4(d)–4(f)). Such difference is summarized in the energy evolution of $3\times3$ peak intensity of both pristine and Ta doped samples (Fig. 4(g)). From 0 meV to 60 meV, the $3\times3$ peak intensity of the pristine $CsV_3Sb_5$ is much higher than that of the Ta doped sample. The concurrent suppression of long-range CDWs and the emergent $3\times3$ charge order indicates the similar origin for these two charge orders.

It should be noted that the stacking of the $2\times2\times2$ CDWs become disordered at 65 K.[49] And the $1\times4$ charge orders disappear at about 60 K.[21] The similar critical temperature

of ∼ 60 K further supports the strong correlation between the emergent 3×3 charge order and the long-range 2×2×2 (1×4) CDWs in the kagome layer. The emergent charge order may result from the hybridization between the periodic surface potential induced by the Cs reconstruction and the underlying 2×2 (1×4) charge orders, although the 3×3 charge order is incommensurate with the bulk charge orders, which is similar to the situation in $RbV_3Sb_5$, where a unidirectional charge order is found on the pristine Rb surface.[48] Furthermore, the Cs atoms will induce an orbital-selective electron doping effect, which might bring a specific band closer to the Fermi level, contributing to the formation of the 3×3 charge order. The emergence of 3×3 charge order on the ordered Cs surface of kagome superconductor $CsV_3Sb_5$ provides new insight for understanding and manipulating the cascade of charge orders in the $AV_3Sb_5$ family. To fully understand the mechanism of the emergent 3×3 charge order, further theoretical investigations are needed.

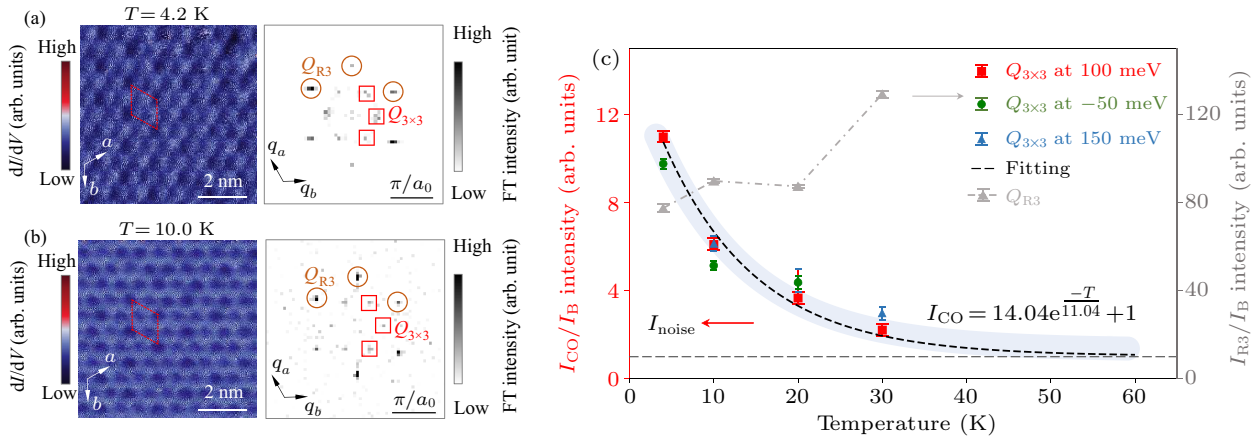


**Fig. 3.** Temperature evolution of 3×3 charge order. (a) and (b) $dI/dV$ maps at −100 mV and corresponding Fourier transform of the same R3 region taken at 4.2 K and 10 K, respectively, showing that the $\boldsymbol{Q}_{3\times3}$ (highlighted by red rectangles) is weakened with increasing temperature. (c) Temperature evolution of the FT intensity of the 3×3 CO at different energies and R3 reconstruction. The data obtained at different energies (marked by distinct color) are included. The FT intensity is defined as $I = I_q/I_{noise}$, where $I_q$ is the averaged intensity of the corresponding order $q$ in three directions in the FT and $I_{noise}$ is the averaged background intensity of the Fourier transform. The blue dashed line is the fitting result by an exponential function. The error bars represent the standard deviation. For all $dI/dV$ data in this figure, $V_{set} = 50$ mV, $I_t = 400$ pA, $V_{mod} = 2$ mV.

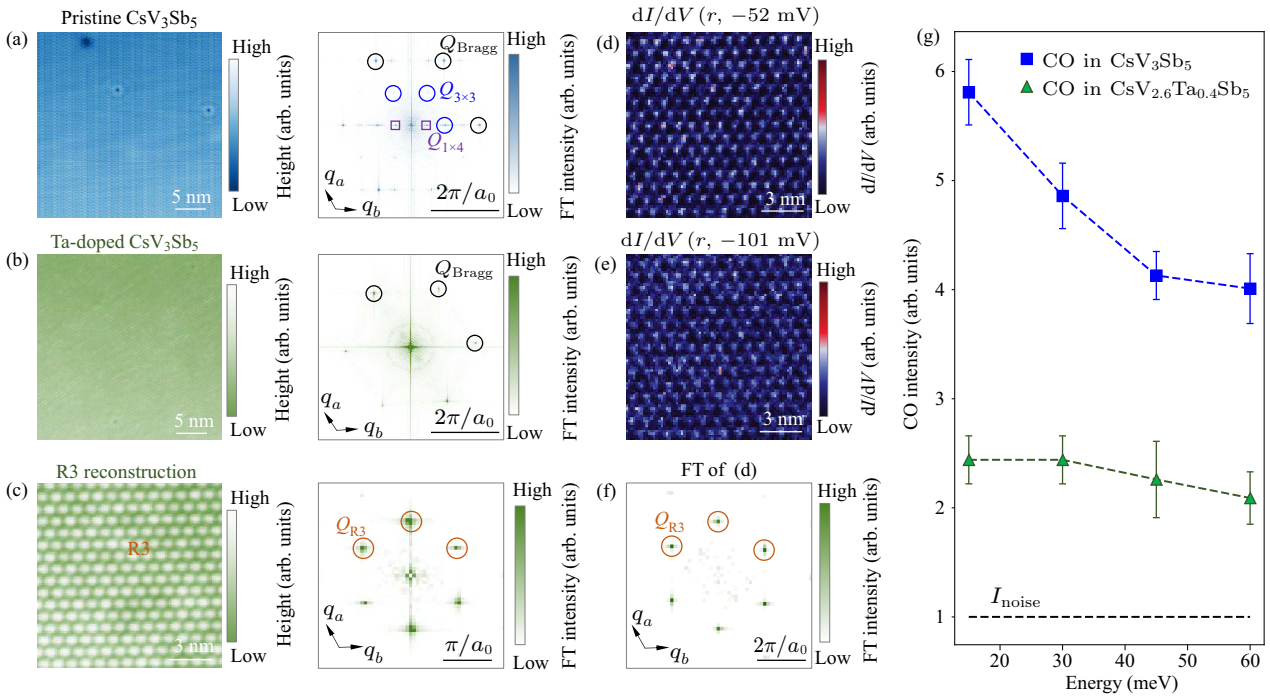


**Fig. 4.** Comparison of charge orders between pristine and Ta doped $CsV_3Sb_5$. (a) STM image and corresponding Fourier transform of the Sb termination of the pristine sample ($V_{set} = 400$ mV, $I_t = 3000$ pA), showing long-range 2×2 (blue circles) and 1×4 (purple squares) CDWs. (b) STM image of the Sb termination of the Ta doped sample $CsV_{2.6}Ta_{0.4}Sb_5$ ($V_{set} = 500$ mV, $I_t = 100$ pA), showing that the long-range CDWs are undetectable. (c) STM image and corresponding FT of the R3 reconstruction in $CsV_{2.6}Ta_{0.4}Sb_5$ ($V_{set} = 900$ mV, $I_t = 50$ pA), showing doping induced non-uniform topographic features. (d) and (e) $dI/dV$ maps at −52 mV and −101 mV of the same region in (c), showing a weakened superlattice modulation. (f) FT of the map in (d), showing blurred signals at the vector of $\boldsymbol{Q}_{3\times3}$. (g) Charge order intensity at different energies in $CsV_3Sb_5$ and $CsV_{2.6}Ta_{0.4}Sb_5$, showing that the CO in $CsV_{2.6}Ta_{0.4}Sb_5$ is significantly suppressed than that in $CsV_3Sb_5$. The error bars represent the standard deviation.

## 4. Conclusions

We observe a 3×3 charge order (CO) with an estimated critical temperature of about 62 K on the R3 Cs ordered surface of pristine $CsV_3Sb_5$. The same reconstruction is observed in the Ta doped sample where the CO is significantly suppressed. The 3×3 charge order is significantly suppressed in the Ta doped $CsV_3Sb_5$, indicating that the emergence of 3×3 charge order on R3 ordered surface is directly correlated with the 2×2×2 (1×4) CDWs in bulk $CsV_3Sb_5$. Our work provides an effective way for creating new quantum states by introducing ordered alkali surface structures in kagome superconductors. And it is also promising to observe new quantum phenomena in other superconductors containing alkali atoms.[26,50,51]

## Acknowledgements

Project supported by the National Key Research and Development Project of China (Grant Nos. 2022YFA1204100 and 2019YFA0308500), the National Natural Science Foundation of China (Grant No. 62488201), the CAS Project for Young Scientists in Basic Research (Grant No. YSBR-003), and the Innovation Program of Quantum Science and Technology (Grant No. 2021ZD0302700).

## References

[1] Starnberg H I, Brauer H E, Holleboom L J and Hughes H P 1993 *Phys. Rev. Lett.* **70** 3111
[2] Adelung R, Brandt J, Rossnagel K, Seifarth O, Kipp L, Skibowski P, Ramírez C, Strasser T and Schattke W 2001 *Phys. Rev. Lett.* **86** 1303
[3] Schmidt P, Murphy B, Kröger J, Jensen H and Berndt R 2006 *Phys. Rev. B* **74** 193407
[4] Lee J, Jin K H and Yeom H W 2021 *Phys. Rev. Lett.* **126** 196405
[5] Miyata Y, Nakayama K, Sugawara K, Sato T and Takahashi T 2015 *Nat. Mater.* **14** 775
[6] Seo J J, Kim B Y, Kim B S, Jeong J K, Ok J M, Kim J S, Denlinger J D, Mo S K, Kim C and Kim Y K 2016 *Nat. Commun.* **7** 11116
[7] Tang C J, Liu C, Zhou G Y, Li F S, Ding H, Li Z, Zhang D, Li Z, Song C L, Ji S H, He K, Wang L L, Ma X C and Xue Q K 2016 *Phys. Rev. B* **93** 020507
[8] Wang Q Y, Li Z, Zhang W H, Zhang Z C, Zhang J S, Li W, Ding H, Ou Y B, Deng P, Chang K, Wen J, Song C L, He K, Jia J F, Ji S H, Wang Y Y, Wang L L, Chen X, Ma X C and Xue Q K 2012 *Chin. Phys. Lett.* **29** 037402
[9] Kyung W S, Huh S S, Koh Y Y, Choi K Y, Nakajima M, Eisaki H, Denlinger J D, Mo S K, Kim C and Kim Y K 2016 *Nat. Mater.* **15** 1233
[10] Zhang W H, Liu X, Wen C H P, Peng R, Tan S Y, Xie B P, Zhang T and Feng D L 2016 *Nano Lett.* **16** 1969
[11] Hossain M A, Mottershead J D F, Fournier D, Bostwick A, McChesney J L, Rotenberg E, Liang R, Hardy W N, Sawatzky G A, Elfimov I S, Bonn D A and Damascelli A 2008 *Nat. Phys.* **4** 527
[12] Fournier D, Levy G, Pennec Y, McChesney J L, Bostwick A, Rotenberg E, Liang R, Hardy W N, Bonn D A, Elfimov I S and Damascelli A 2010 *Nat. Phys.* **6** 905
[13] Sierda E, Huang X, Badrtdinov D I, Kiraly B, Knol E J, Groenenboom G C, Katsnelson M I, Rösner M, Wegner D and Khajetoorians A A 2023 *Science* **380** 1048
[14] Hu Q X, Yang F Z, Wang X Y, Li J J, Liu W Y, Kong L Y, Li S L, Yan L, Xu J P and Ding H 2023 *Phys. Rev. Mater.* **7** 034801
[15] Hu B, Ye Y, Huang Z, Han X, Zhao Z, Yang H, Chen H and Gao H J 2022 *Chin. Phys. B* **31** 058102
[16] Tan H X, Liu Y, Wang Z and Yan B 2021 *Phys. Rev. Lett.* **127** 046401
[17] Ortiz B R, Gomes L C, Morey J R, Winiarski M, Bordelon M, Mangum J S, Oswald L W H, Rodriguez-Rivera J A, Neilson J R, Wilson S D, Ertekin E, McQueen T M and Toberer E S 2019 *Phys. Rev. Mater.* **3** 094407
[18] Yin Q W, Tu Z J, Gong C S, Fu Y, Yan S H and Lei H C 2021 *Chin. Phys. Lett.* **38** 037403
[19] Park T, Ye M X and Balents L 2021 *Phys. Rev. B* **104** 035142
[20] Denner M M, Thomale R and Neupert T 2022 *Phys. Rev. Lett.* **128** 099901
[21] Zhao H, Li H, Ortiz B R, Teicher S M L, Park T, Ye M, Wang Z, Balents L, Wilson S D and Zeljkovic I 2021 *Nature* **599** 216
[22] Jiang Y, Yu Z, Wang Y, Lu T, Meng S, Jiang K and Liu M 2022 *Chin. Phys. Lett.* **39** 047402
[23] Wu P, Tu Y B, Wang Z Y, Yu S K, Li H Y, Ma W R, Liang Z W, Zhang Y M, Zhang X C, Li Z Y, Yang Y, Qiao Z H, Ying J J, Wu T, Shan L, Xiang Z J, Wang Z Y and Chen X H 2023 *Nat. Phys.* **19** 1143
[24] Nie L P, Sun K, Ma W R, Song D W, Zheng L X, Liang Z W, Wu P, Yu F H, Li J, Shan M, Zhao D, Li S J, Kang B L, Wu Z M, Zhou Y B, Liu K, Xiang Z J, Ying J J, Wang Z Y, Wu T and Chen X H 2022 *Nature* **604** 59
[25] Asaba T, Onishi A, Kageyama Y, Kiyosue T, Ohtsuka K, Suetsugu S, Kohsaka Y, Gaggl T, Kasahara Y, Murayama H, Hashimoto K, Tazai R, Kontani H, Ortiz B R, Wilson S D, Li Q, Wen H H, Shibauchi T and Matsuda Y 2024 *Nat. Phys.* **20** 40
[26] Yang H, Ye Y, Zhao Z, Liu J, Yi X W, Zhang Y, Shi J, You J Y, Huang Z,Wang B,Wang J, Guo H, Lin X, Shen C, ZhouW, Chen H, Dong X, Su G, Wang Z and Gao H J 2024 *Nat. Commun.* **15** 9626
[27] Hu Y, Le C C, Zhang Y H, Zhao Z, Liu J L, Ma J Z, Plumb N C, Radovic M, Chen H, Schnyder A P, Wu X X, Dong X L, Hu J P, Yang H T, Gao H J and Shi M 2023 *Nat. Phys.* **19** 1827
[28] Li H, Zhao H, Ortiz B R, Park T, Ye M X, Balents L, Wang Z Q, Wilson S D and Zeljkovic I 2022 *Nat. Phys.* **18** 265
[29] Li H, Zhao H, Ortiz B R, Oey Y, Wang Z Q, Wilson S D and Zeljkovic I 2023 *Nat. Phys.* **19** 637
[30] Chen H, Yang H, Hu B, Zhao Z, Yuan J, Xing Y, Qian G, Huang Z, Li G, Ye Y, Ma S, Ni S, Zhang H, Yin Q, Gong C, Tu Z, Lei H, Tan H, Zhou S, Shen C, Dong X, Yan B, Wang Z and Gao H J 2021 *Nature* **599** 222
[31] Zhou S and Wang Z 2022 *Nat. Commun.* **13** 7288
[32] Chen H and Gao H J 2023 *Nature* **618** 910
[33] Chen H, Hu B, Ye Y, Yang H and Gao H J 2022 *Chin. Phys. B* **31** 097405
[34] Ortiz B R, Teicher S M L, Hu Y, Zuo J L, Sarte P M, Schueller E C, Abeykoon A M M, Krogstad M J, Rosenkranz S, Osborn R, Seshadri R, Balents L, He J and Wilson S D 2020 *Phys. Rev. Lett.* **125** 247002
[35] Ni S L, Ma S, Zhang Y H, Yuan J, Yang H T, Lu Z Y W, Wang N N, Sun J P, Zhao Z, Li D, Liu S B, Zhang H, Chen H, Jin K, Cheng J G, Yu L, Zhou F, Dong X L, Hu J P, Gao H J and Zhao Z X 2021 *Chin. Phys. Lett.* **38** 057403
[36] Yang H T, Huang Z H, Zhang Y H, Zhao Z, Shi J N, Luo H L, Zhao L, Qian G J, Tan H X, Hu B, Zhu K, Lu Z Y W, Zhang H, Sun J P, Cheng J G, Shen C M, Lin X, Yan B H, Zhou X J, Wang Z Q, Pennycook S J, Chen H, Dong X L, Zhou W and Gao H J 2022 *Sci. Bull.* **67** 2176
[37] Luo Y, Han Y L, Liu J J, Chen H, Huang Z H, Huai L W, Li H Y, Wang B Q, Shen J C, Ding S H, Li Z Y, Peng S T, Wei Z Y, Miao Y, Sun X P, Ou Z P, Xiang Z J, Hashimoto M, Lu D H, Yao Y G, Yang H T, Chen X H, Gao H J, Qiao Z H, Wang Z W and He J F 2023 *Nat. Commun.* **14** 3819
[38] Zhao Z, Wang R, Zhang Y, Zhu K, Yu W, Han Y, Liu J, Hu G, Guo H, Lin X, Dong X, Chen H, Yang H and Gao H J 2024 *Chin. Phys. B* **33** 077406
[39] Hu B, Chen H, Ye Y, Huang Z, Han X, Zhao Z, Xiao H, Lin X, Yang H, Wang Z and Gao H J 2024 *Nat. Commun.* **15** 6109
[40] Huang Z H, Han X, Zhao Z, Liu J, Li P, Tan H, Wang Z, Yao Y, Yang H, Yan B, Jiang K, Hu J, Wang Z, Chen H and Gao H J 2024 *Sci. Bull.* **69** 885
[41] Liang Z, Hou X, Zhang F, Ma W, Wu P, Zhang Z, Yu F, Ying J J, Jiang K, Shan L, Wang Z and Chen X H 2021 *Phys. Rev. X* **11** 031026

[42] Song B, Ying T, Wu X, Xia W, Yin Q, Zhang Q, Song Y, Yang X, Guo J, Gu L, Chen X, Hu J, Schnyder A P, Lei H, Guo Y and Li S 2023 *Nat. Commun.* **14** 2492
[43] Huang Z H, Han X H, Zhao Z, Yang H T, Chen H and Gao H J 2024 *Nano. Lett.* **24** 6023
[44] Kato T, Li Y K, Liu M, Nakayama K, Wang Z W, Souma S, Kitamura M, Horiba K, Kumigashira H, Takahashi T, Yao Y G and Sato T 2023 *Phys. Rev. B* **107** 245143
[45] Kato T, Li Y K, Nakayama K, Wang Z W, Souma S, Kitamura M, Horiba K, Kumigashira H, Takahashi T and Sato T 2022 *Phys. Rev. B* **106** L121112
[46] Nakayama K, Li Y K, Kato T, Liu M, Wang Z W, Takahashi T, Yao Y G and Sato T 2022 *Phys. Rev. X* **12** 011001
[47] Kato T, Nakayama K, Li Y K, Wang Z W, Sugawara K, Tanaka K, Takahashi T, Yao Y G and Sato T 2024 *Adv. Sci.* **11** 2309003
[48] Yu J, Xu Z, Xiao K, Yuan Y, Yin Q, Hu Z, Gong C, Guo Y, Tu Z, Tang P, Lei H, Xue Q K and Li W 2022 *Nano Lett.* **22** 918
[49] Jin F, Ren W, Tan M S, Xie M T, Lu B R, Zhang Z, Ji J T and Zhang Q M 2024 *Phys. Rev. Lett.* **132** 066501
[50] Hardy F, Eder R, Jackson M, Aoki D, Paulsen C, Wolf T, Burger P, Böhmer A, Schweiss P, Adelmann P, Fisher R A and Meingast C 2014 *J. Phys. Soc. Jpn.* **83** 014711
[51] Cao L, Liu W, Li G, Dai G, Zheng Q, Wang Y, Jiang K, Zhu S, Huang L, Kong L, Yang F, Wang X, Zhou W, Lin X, Hu J, Jin C, Ding H and Gao H J 2021 *Nat. Commun.* **12** 6312